212 GOPS Programmable Large Scale Hopfield-Inspired Integrated Photonic Ising Machine enabled by DSP

Charles St-Arnault[1,*], Nayem AL-Kayed[2,*], Hugh Morison[2,*], Aadhi Al-Rahim[2,3], Alexander N. Tait[2], David V. Plant[1] and Bhavin J. Shastri[2]

[1] *Dept. of Electrical and Computer Engineering, McGill University, Montreal, QC, Canada*
[2] *Dept. of Electrical and Computer Engineering, Queen's University, Kingston, ON, Canada*
[3] *Dept. of Optics and Photonics, Indian Institute of Technology, Delhi 110016, India*

**Authors contributed equally*
charles.st-arnault@mail.mcgill.ca

Abstract: We report a DSP enabled programmable, record scale and speed photonic Ising machine operating at 212 GOPS with best-in-class solution quality for Max-Cut problems and ground state solutions for protein folding problems. © 2026 The Author(s)

1. Introduction

The Ising model, now 100 years old [1], was initially formulated to explore the combined behavior of magnetic spins. It is now broadly applied across various fields, such as solid state and statistical problems, quantum information, drug discovery and more [2]. Nondeterministic polynomial (NP) problems, such as prime number factorization and the tried-and-true problem of the optimal route of the traveling salesman, are examples of the most challenging computational problems, defined by their computational complexity. Executing drug discovery via protein folding, another NP problem, would reduce medical drug development cost and time. However, these problems remain out of reach even for modern supercomputers because the problem size scales exponentially with the variable count [3]. Fortunately, NP problems can be solved by mapping the problem to the Ising model represented by a graph of binary spins (σ_i) (vertices) and spin-to-spin interactions (J_{ij}) (edges) with an assigned coupling strength [4]. Relevant NP problems solved with the Ising model require matrices with tens of millions of elements to be implemented. Conventional Ising solvers utilize digital hardware (e.g., computing clusters), demanding substantial computational resources and energy to perform the immense matrix multiplications required [5]. Unconventional Ising computing platforms instead implement this model using diverse physical systems such as, quantum annealers, electromechanical oscillators, and more [5], but are greatly limited by bandwidth, scalability, and stability. The recently proposed photonic Ising machines instead use photons to represent the spin states and to perform the matrix multiplication. Using the photonic platform enables a high-speed and energy-efficient computing platform [6]. However, existing state-of-the-art photonic Ising machine based on optoelectronic parametric oscillator and spatial light modulators [7, 8], suffer from stability issues and challenges in controlling a large number of physical parameters, restricting their practical applications in advanced computation to small scale problems. In this work, we demonstrate a programmable photonic Ising machine featuring up to 256 all-to-all connected spins (65,536 couplings) or 41,209 sparsely connected spins (205,233 couplings) operating at 212 giga-operations per second (GOPS) achieving the highest solution quality for Max-Cut problems, and ground state solutions for protein folding problems.

2. Ising Model Framework

An N-spin Ising problem is solved by finding the spins configuration ($\sigma_i \in \pm 1$) that minimizes the Hamiltonian:

$$H = \sum_{i<j} J_{ij}\sigma_i\sigma_j + \sum_i h_i\sigma_i \tag{1}$$

The specific problem is defined by its $N \times N$ coupling matrix J and the local bias h. For the energy to be minimized, the spins must converge to ± 1 in the proper order, at which point the optimal solution is reached. The iterative gradient descent on the Ising Hamiltonian is performed with the continuous spin variable $\sigma_i = sign(\mathbf{x_i})$, where $\mathbf{x} \in \mathbb{R}$. This can be approximated with a bounded sinusoidal function (e.g., Mach-Zehnder modulator (MZM) transfer function). At each iteration, the state is updated with the current state and the gradient of the Hamiltonian:

$$\begin{aligned}\mathbf{x}^{(t+1)} &= \alpha\mathbf{x}^{(t)} - \beta\nabla_x H \\ &\approx (\alpha\mathbf{I} - \beta\mathbf{J})\cdot\sigma(\mathbf{x}^{(t)}) - \beta\mathbf{h}\end{aligned} \tag{2}$$

Hyperparameters α and β govern the feedback and coupling strength and closely impact the convergence of the system. This state update can be expressed as a matrix-vector multiplication operation by concatenating the local bias $-\beta h$ with the weight matrix $W = \alpha I - \beta J$, and adding a value of 1 to the vector $\mathbf{x}$:

$$\mathbf{W} = [\alpha\mathbf{I} - \beta\mathbf{J}| - \beta\mathbf{h}] \quad \text{and} \quad \mathbf{x}'^T = [\mathbf{x}^T|1],\ \mathbf{x}^{(t+1)} = \mathbf{W}\cdot\sigma(\mathbf{x}'^{(t)}) + n(\zeta) \tag{3}$$

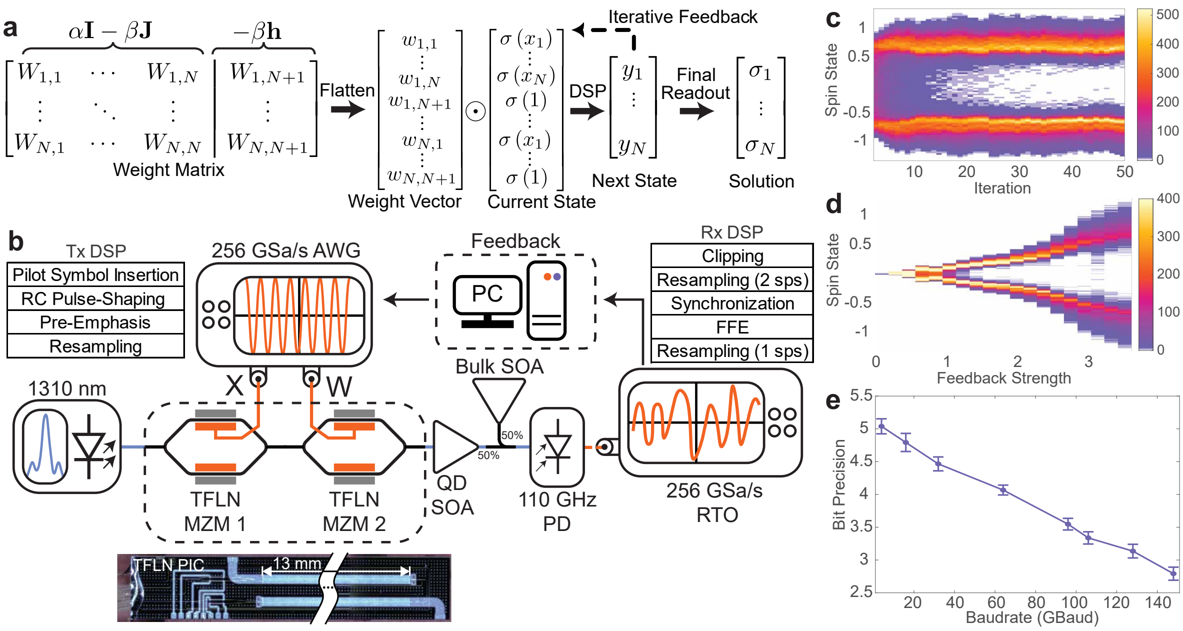

Fig. 1: (a) Mathematical framework illustrating the photonic Ising machine principle. (b) Experimental setup and DSP stacks used for the photonic Ising machine. (c) Heatmap showing the evolution of uncoupled spins over successive iterations at a feedback strength of $\alpha = 3.5$. (d) Heatmap of the bifurcation dynamics as a function of feedback strength at 64 Gbaud with $N = 262144$ uncoupled spins. (e) Bit-precision of a 128×128 analog matrix-vector multiplication as the symbol rate increases from 4 to 148 Gbaud.

Where $n(\zeta)$ represents a gaussian noise term of variance ζ^2 adding stochasticity. The matrix-vector multiplication can be performed using time-domain multiplexed element wise vector-vector multiplication as shown in Fig. 1 (a). The weight matrix is flattened into a a 1D vector. The current state spin configuration is repeated N-times to match the 1D weight vector size. Element wise multiplication between weights and spin states is performed in the optical domain using two cascaded MZMs. DSP stacks are applied to the resulting spin state, which is iteratively fed back as the current state. At the last iteration, the solution can be read from the final spin state.

3. Experimental Setup and DSP Stacks

Fig. 1 (b) shows the experimental setup and DSP stacks used for our photonic Ising machine. Cascaded thin-film lithium niobate (TFLN) modulators with 3-dB bandwidths larger than 110 GHz and 1.5V low-MHz V_π are used to perform the element-wise multiplication described in the previous section. Both modulators are biased at quadrature, while TFLN MZM 1 is driven with a near V_π peak-to-peak voltage to utilize its non-linear transfer function. The current state and weight matricies are generated by a 256 GSa/s waveform generator. After flattening the W matrix, and repeating the current state vector (as described in the previous section), a sequence of PAM8 pilot symbols are inserted into both the state and weight matrices. Those pilots serve as a mean to synchronize the signal at the receiver, and adapt the feed-forward equalizer tap coefficients, as blind equalization is not suited for analog multiplication. Raised-cosine pulse-shaping is used to restrict the signal bandwidth, and pre-emphasis is used to compensate for the waveform generator frequency response. The signal is then resampled to obtain the desired symbol rate and the electrical signal is generated. The element-wise multiplied signal then occurs in the optical domain, and is amplified by a high-performance quantum-dot (QD) semiconductor optical amplifier (SOA) [9]. To add stochasticity ($n(\zeta)$), a high noise figure (7 dB) bulk SOA is used as an approximate gaussian noise source. The amount of injected noise is controlled by the SOA bias current enabling noise annealing during problem solving. Finally, the signal is recovered with a 110 GHz photodiode and sampled by a 256 GSa/s real-time oscilloscope. Clipping is then applied to the signal in order to reduce the peak-to-average power ratio (PAPR), which if too high, can drastically reduce the solver's performance against selected problems. Since this machine operates with feedback over many iterations, clipping on the receiver side directly impacts the transmitted signal PAPR at the next iteration. The signal is synchronized and the adapted FFE taps are convolved with the signal. The signal is resampled to 1 sample-per-symbol, and the next-state can be read or fed back to the next iteration.

4. Results and discussion

Fig. 1 (c)-(d) show the bifurcation dynamics at 64 Gbaud as a function of iteration count (c) and feedback strength (d). To obtain proper bifurcation, a feedback strength of 3.5 was required to overcome the system attenuation. Fig. 1 (e) shows the bit-precision of a matrix-vector multiplication as a function of symbol rate. At 4 Gbaud, a 5-bit precision is obtained, while at 148 Gbaud, due to system impairements (bandwidth limitations, V_π function of frequency, noise, etc.) the bit-precision is reduced to 2.8. Notwitstanding, in the context of Ising machines, such system-wide distortions can be helpful to escape local minima by acting as a form of annealing. At a symbol rate of 106 Gbaud, the system achieves 3.3-bit precision and a processing speed of 212 GOPS, nearly twice

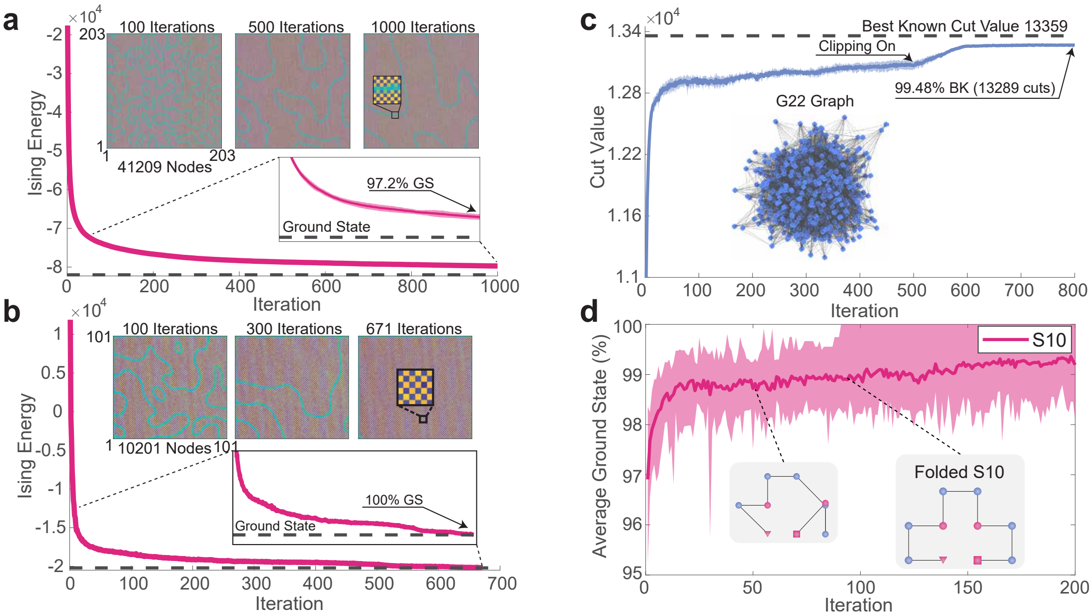

Fig. 2: All problems run at 212 GOPS: (a–b) 41,209–10,201 node 2D lattice, (c) Max-Cut G22, (d) S10 HP protein folding.

the previous record for photonic matrix–vector multiplication [10]. All subsequent results use 106 Gbaud (212 GOPS). Fig. 2 (a)-(b) show 2D square lattice problems of 41,209 spins (205,233 couplings) and 10,201 spins (50,601 couplings) respectively. Our photonic Ising machine demonstrates the largest spin configuration reported to date for optoelectronics oscillator based Ising machines. The 41,209 spin square lattice, achieves 97.2% of the ground state solution after 1000 iterations. As shown in the insets, the system initially forms small spin domains that coalesce into a pure checkerboard as the energy approaches ground state. Our simulations indicate that the problem would reach ground state after 5,366 iterations. The 10,201 spin 2D lattice achieved ground state at 671 iterations. Fig. 1 (c) shows the Max-Cut G22 problem results. Our system achieved on average 99.48% of the best known solution value, which surpass prior photonic Ising machine reported results [11]. The G22 problems suffers from particularly high PAPR values in the time domain state vector. Applying clipping starting at the 500th iteration led to a marked improvement in convergence. As shown in the figure, a sharp increase in the cut value occurs immediately after clipping is enabled. Clipping reduces the PAPR, which makes for a better utilization of the overall system bit-resolution, and maximal drive voltage leading to better MZM non-linearity extraction and better analogue performance, both improving amplitude inhomogeneity. Fig. 2 (d) shows an 10 amino acid HP protein structure (S_{10}) folded by our photonic Ising machine. The task is to predict the stable structure a chain of amino acids will adopt (a problem with an exponential growing solution space). Deep learning models, such as Alphafold 3, have shown promise. The HP lattice model provides a complementary, physics based approach. It classifies the amino acids as hydrophobic (H) or polar (P) and seeks the lowest-energy configuration by maximizing H–H interactions, framing structure prediction as an optimization problem. Fig. 2 (d) shows the solution quality evolution for the S_{10} sequence. The ground state was achieved 40% of the runs over 10 runs, with around 100 iterations required on average. The mean solution quality across all 10 runs was 99%.

5. Conclusion

We demonstrated a DSP enabled photonic Ising machine based on a cascaded MZM architecture operating at 212 GOPS showcasing record scale and operational speed, best-in-class solution quality and ground state solutions for real-life problems such as protein folding.

References

1. E. Ising, "Beitrag zur theorie des ferromagnetismus," *Z. Physik*, vol. 31, pp. 253–258, 1925.
2. Z. Budrikis, "100 years of the Ising model," *Nat. Rev. Phys.*, vol. 6, p. 530, 2024.
3. D. S. Hochba, "Approximation algorithms for NP-hard problems," *ACM Sigact News*, vol. 28, pp. 40–52, 1997.
4. B. A. Cipra, "The Ising model is NP-complete," *SIAM News*, vol. 33, pp. 1–3, 2000.
5. N. Mohseni, P. L. McMahon, and T. Byrnes, "Ising machines as hardware solvers of combinatorial optimization problems," *Nat. Rev. Phys.*, vol. 4, pp. 363–379, 2022.
6. Y. Shen et al., "Deep learning with coherent nanophotonic circuits," *Nat. photonics*, vol. 11, pp. 441–446, 2017.
7. T. Honjo et al., "100,000-spin coherent Ising machine," *Sci. Adv.*, vol. 7, eabh0952, 2021.
8. D. Pierangeli, G. Marcucci, and C. Conti, "Large-scale photonic Ising machine by spatial light modulation," *Phys. review letters*, vol. 122, p. 213 902, 2019.
9. C. St-Arnault et al., "Performance and Characterization Comparison of QD SOA, QW SOA, Bulk SOA and PDFA for Multi-Tbps O-Band WDM Links," *J. Light. Technol.*, vol. 43, no. 4, pp. 1915–1925, 2025.
10. Z. Lin et al., "120 GOPS photonic tensor core in thin-film lithium niobate for inference and in situ training," *Nat. Commun.*, vol. 15, p. 9081, 2024.
11. Y. Gao, G. Chen, L. Qi, W. Fu, Z. Yuan, and A. J. Danner, "Photonic Ising machines for combinatorial optimization problems," *Appl. Phys. Rev.*, vol. 11, no. 4, 2024.